Available online at www.sciencedirect.com
ScienceDirect
Journal of Solid State Chemistry 179 (2006) 3007–3016
JOURNAL OF SOLID STATE CHEMISTRY
www.elsevier.com/locate/jssc

From thorium phosphate hydrogenphosphate hydrate to β-thorium phosphate diphosphate: Structural evolution to a radwaste storage ceramic

Gilles Wallez[a,*], Nicolas Clavier[b], Nicolas Dacheux[b], Michel Quarton[a], Wouter van Beek[c]

[a]*Université Pierre et Marie Curie-Paris 6, CNRS UMR 7574, Chimie de la Matière Condensée de Paris, 4 place Jussieu, Paris F-75005, France*
[b]*Groupe de Radiochimie, IPN, Université Paris-Sud-11, Orsay F-91406, France*
[c]*European Synchrotron Radiation Facility, 6 rue Jules Horowitz, BP 220, Grenoble F-38043, France*

Received 31 March 2006; received in revised form 19 May 2006; accepted 20 May 2006
Available online 3 June 2006

Abstract

β-Thorium phosphate diphosphate (β-TPD), considered as a very promising radwaste storage material, was obtained from thorium phosphate hydrogenphosphate hydrate (TPHPH) precursor through dehydration and hydrogen phosphate condensation. The structures of TPHPH, intermediate α-thorium phosphate diphosphate (α-TPD) and its hydrate (α-TPDH) have been resolved ab initio by Rietveld analysis of their synchrotron diffraction patterns. All were found orthorhombic (space group *Cmcm*) and similarly composed of $[ThPO_4]_4^{4+}$ slabs alternating with disordered layers hosting either $[HPO_4 \cdot H_2O]_2^{4-}$ (TPHPH), $[P_2O_7 \cdot 2H_2O]^{4-}$ (α-TPDH), or $[P_2O_7]^{4-}$ (α-TPD), unlike the 3D structure of β-TPD. The diphosphate groups of α-TPD and α-TPDH are strongly bent. The irreversible transition to the final β-TPD consists in a shearing of the slabs and a reduction of the interslabs cavities that explains the stability of this high-temperature form.

Keywords: Actinide phosphate; Radwaste storage; Synchrotron diffraction; Inorganic structures

1. Introduction

Since the mid-1990s, a considerable deal of studies have been dedicated to the search of host matrices for actinides, in the scope of immobilizing high-radioactive long-life radwaste such as radionuclides coming from an advanced reprocessing of the spent fuel, or excess plutonium from dismantled nuclear weapons. In this scope, the French national research group NOMADE has initiated a multi-disciplinary program of evaluation that allowed to select several host ceramics and composites for their high chemical durability, low aqueous solubility and resistance to radiation damage [1]. Among them, $Th_4(PO_4)_4P_2O_7$ (TPD) shows excellent performances with the possibility to substitute Th^{4+} cation by large amounts of smaller ones like U^{4+}, Np^{4+}, Pu^{4+} (respectively, up to 75, 52, 41 mol%) [2–5]. This promising material can be prepared either by dry or wet chemical routes, involving the initial precipitation of low-temperature precursors: this method appears as the most convenient for the elaboration of solid solutions containing both thorium and other actinides, since it provides a more homogeneous distribution of the cations in the material [6,7]. Moreover, the very low solubility of the precursor allows considering the quantitative decontamination of low- and high-level radioactive liquid waste containing actinides through precipitation processes [8].

Indeed, the precipitation in close container of a stoïchiometric mixture of concentrated $ThCl_4$ solution and 5 M H_3PO_4 yields to the crystallized thorium phosphate hydrogenphosphate hydrate, ($Th_4(PO_4)_4(HPO_4)_2 \cdot 2H_2O$, TPHPH), which is then heated up to 1050–1250 °C to obtain the final ceramic. Recently, we reported a

*Corresponding author. Fax. +33 1 44 27 25 48.
E-mail address: gw@ccr.jussieu.fr (G. Wallez).

0022-4596/$ - see front matter © 2006 Elsevier Inc. All rights reserved.
doi:10.1016/j.jssc.2006.05.027

combined study of the thermal evolution of TPHPH by high-temperature XRD, NMR, EPMA, TGA/DSC, IR and μ-Raman spectroscopy [9], showing the successive phase transitions (Fig. 1):

- TPHPH dehydrates reversibly around 180 °C to TPHP (anhydrous thorium phosphate hydrogenphosphate, $Th_4(PO_4)_4(HPO_4)_2$);
- short above 230 °C, the hydrogenphosphate groups of TPHP condense irreversibly into diphosphates, leading to α-TPD (α-thorium phosphate diphosphate, $Th_4(PO_4)_4P_2O_7$);
- left in air at room temperature, α-TPD re-hydrates promptly into α-TPDH (α-thorium phosphate diphosphate hydrate, $Th_4(PO_4)_4P_2O_7 \cdot nH_2O$);
- around 950 °C, α-TPD turns irreversibly into β-TPD (β-thorium phosphate diphosphate, $Th_4(PO_4)_4P_2O_7$), previously known as TPD in the literature. This final TPD form appears very stable and immune from re-hydratation. Its crystal structure, resolved as soon as 1996, is orthorhombic *Pcam* with cell parameters $a = 12.8646(9)$ Å, $b = 10.4374(8)$ Å, $c = 7.0676(5)$ Å ($V = 949.0(1)$ Å^3, $Z = 2$) [10].

The crystal structures of the other compounds are unpublished, except for a rough model for TPHPH recently proposed by Salvado et al. [11]. High-temperature XRD has shown a strong similarity between TPHPH, TPHP, α-TPD and α-TPDH, but excepting the *c*-cell parameters, neither their patterns nor their cells (orthorhombic *C*, typically $a = 21.4$ Å, $b = 6.7$ Å, $c = 7.0$ Å, $V = 1005$ Å^3) show clear relations with those of β-TPD [9]. Another unexplained difference of considerable importance regarding the applications lied in the textures of these materials: whereas TPHPH is soft and foliated [9], β-TPD can be sintered as a ceramic. Likewise, the stability of the β-form, suggested by the irreversibility of the α–β transition, had to be duly established through the determination of the crystal structures of TPHPH, α-TPD and α-TPDH. Note that TPHP was excluded from this study due to the closeness and the spreading of the TPHPH/TPHP and TPHP/α-TPD transitions that do not allow preparing this intermediate form pure enough.

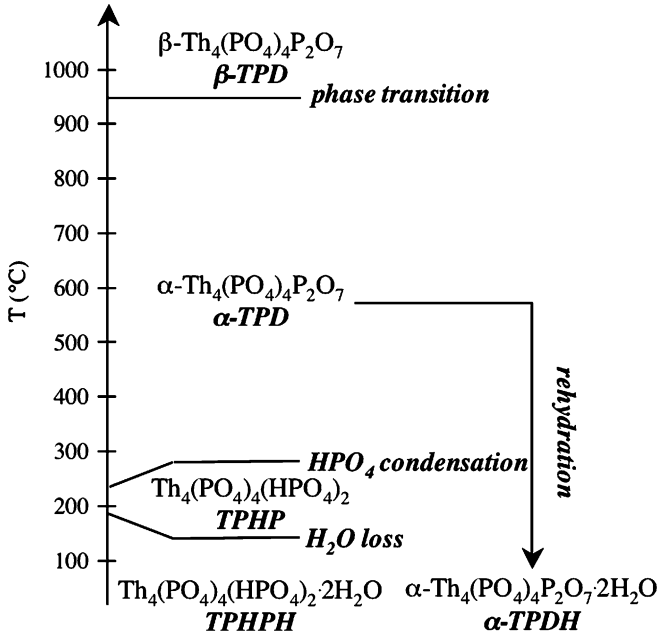

Fig. 1. Thermal evolution scheme for TPHPH.

2. Experimental section

The TPHPH sample used as starting material for these studies was prepared following the wet chemistry route described above [6,7]. Both powder diffraction and Electron Probe MicroAnalysis (EPMA, using $SmPO_4$ and ThO_2 as calibration standards) experiments confirmed that the solid was homogeneous and single phase [9].

2.1. Thermogravimetric analysis

In a preliminary study, cyclic DTA/TGA of α-TPDH were performed in air on a Setaram TG 92-16 apparatus with a 120 °C h^{-1} heating/cooling rate in order to evaluate the number of water molecules in this compound. Two phenomena were evidenced (Fig. 2):

- the diffuse mass loss starting from 50 °C on heating, reached 1.1–1.9% depending on the sample and was attributed to the evaporation of adsorbed water; the reverse phenomenon was not observed, probably because of an associated slow kinetics;
- although the two losses overlap each other, the second one appears sharper and fully reversible during cooling and subsequent cycles then can be quantified. This 2.3% loss, also pointed out by DTA, occurs between 190 and 300 °C. It corresponds to two water molecules per $Th_4(PO_4)_4P_2O_7$ unit (2.37% in theory), leading to $Th_4(PO_4)_4P_2O_7 \cdot 2H_2O$ as the probable formula for the hydrated α-TPDH compound. When cooling, the compound rehydrates from 260 °C on, accounting for strongly bonded structural water molecules.

2.2. Synchrotron diffraction

Since single-crystals of these compounds were never obtained (except for β-TPD [10]), all the studies were carried out on powders. TPHPH and α-TPDH have been introduced into 0.3 mm glass capillaries. α-TPD, very prone to re-hydration, was directly prepared in its capillary from a second α-TPDH sample heated for 2 h at 400 °C, then immediately sealed. After recording on the BM01B line of the European Synchrotron Radiation Facility (Grenoble, France), the diffracted intensities were combined into

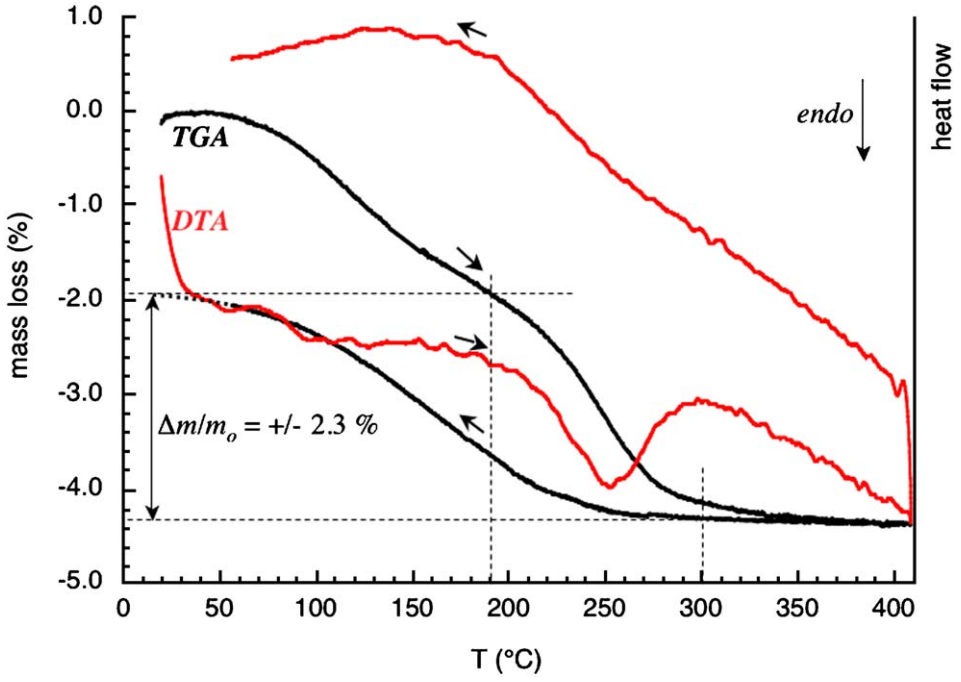

Fig. 2. DTA/TGA plot for α-TPDH.

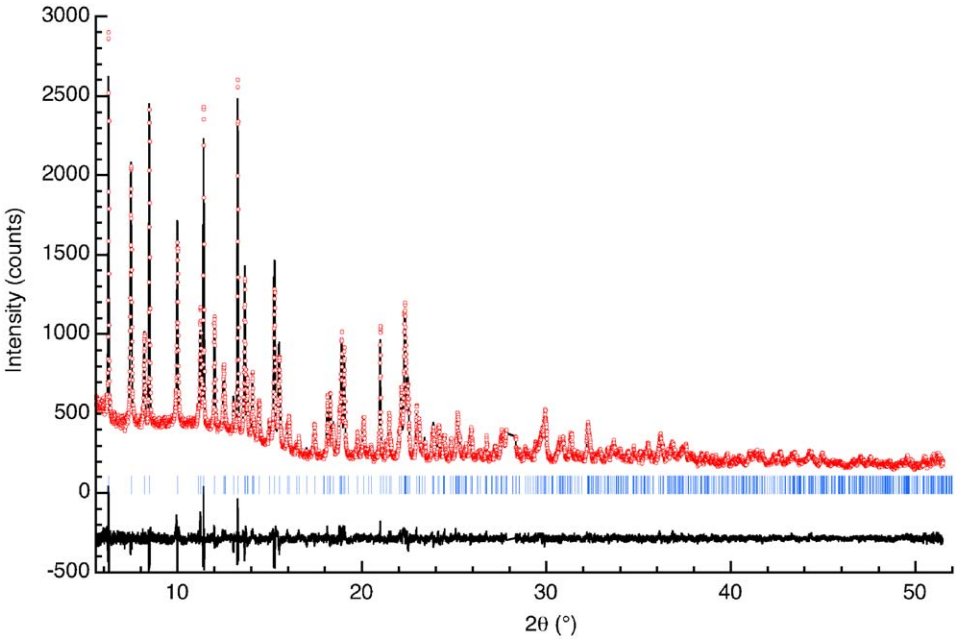

Fig. 3. Rietveld plot for TPHPH: I_{obs} (circles), I_{cal} (solid), Bragg positions (bars) and I_{obs}–I_{cal} (solid, lower).

0.006° bins for Rietveld analysis. Fig. 3 shows the Rietveld plot for TPHPH. Operating and analysis conditions are reported in Table 1.

Using instrumental parameters refined previously from a LaB_6 pattern, the Rietveld analysis in profile-matching mode, performed with Fullprof.2k [12] confirmed the orthorhombic cells already reported [9]. The intensities were extracted and corrected from absorption, considering a 20% compactness as measured by weighting the capillaries.

The platelet habit of the crystallites [9] generated a broadening of the *h*-dependent peaks and a slight orientation effect on the intensities that were taken into account. Systematic extinctions showed a *C*-lattice and a *c*-glide mirror perpendicular to *b*. The density measurements [9] accounted for two $Th_4(PO_4)_4(HPO_4)_2 \cdot 2H_2O$ (or equivalent) unit formulae per cell.

A Patterson synthesis performed with SHELX-97 [13] allowed locating the thorium atoms. The analysis of the Fourier maps [14] of the three compounds revealed dense

Table 1
Data collection, refinement conditions and crystallographic data for TPHPH, α-TPD and α-TPDH

	TPHPH	α-TPD	α-TPDH
Data collection for			
Temperature	293 K		
Apparatus	ESRF-BM01B		
Wavelength	0.69947 Å	0.50007 Å	0.69947 Å
Monochromator	(111) Si (rear)	(111) Si (rear)	(111) Si (rear)
2θ scan limits, step	4.06–55.50°, 0.006°	5.56–45.50°, 0.006°	4.06-51.50°, 0.006°
Observed reflections	725	1133	598
Refinement conditions for			
I-dependent parameters	37	32	35
Background fitting	Interpolation between selected points		
Profile model	Thompson–Cox–Hastings with anisotropic size effect		
$R_P = \Sigma\|y_o^i - y_c^i\|/\Sigma y_o^i$	0.038	0.042	0.036
R_{WP} (id., weighted)	0.049	0.055	0.045
$R_{Bragg} = \Sigma\|I_o^i - I_c^i\|/\Sigma I_o$	0.039	0.032	0.027
$R_{exp} = ((n-p)/\Sigma w_i y_o^i)^{1/2}$	0.027	0.042	0.039
$R_F = \Sigma\|(I_o^i)^{1/2} - (I_c^i)^{1/2}\|/\Sigma(I_o^i)^{1/2}$	0.032	0.020	0.019
$\chi^2 = (R_{wp}/R_{exp})^2$	1.4	1.7	1.4
Crystallographic data for			
Formula	$Th_4(PO_4)_4(HPO_4)_2 \cdot 2H_2O$	$Th_4(PO_4)_4(P_2O_7)$	$Th_4(PO_4)_4(P_2O_7).2H_2O$
System, space group	Orthorhombic, *Cmcm* (63)		
a (Å)	21.4201(2)	21.4205(2)	21.4168(2)
b (Å)	6.69826(5)	6.69180(4)	6.69080(5)
c (Å)	7.03348(4)	7.02925(4)	7.02710(5)
V (Å^3)	1009.14(2)	1007.59(2)	1006.95(2)
Z, formula weight (g mol^{-1}), calc. density	2, 1536, 5.06	2, 1482, 4.88	2, 1518, 5.01

$[Th_4(PO_4)_4]^{4+}$ slabs extending parallel to the (*b*,*c*) plane. These atoms, as well as the residual electron density, obeyed to *m*-mirrors perpendicular to *a* and *c*, the Th, P(1) and some O atoms being located on the second one. For instance, an attempt of refinement in the *Cc* space group yielded in differenciated positions of Th atoms only 0.03(1) Å apart from their sites in *Cmcm* and complying with the (001) *m*-mirror ($\Delta z = 0.003(6)$), thus leading to adopt the latter space group.

3. Results

As could be inferred from their powder patterns, the three compounds show a remarkable similarity in the structure of their $[Th_4(PO_4)_4]^{4+}$ slabs. The thorium atom is bonded to six oxygen atoms of the P(1)O_4 groups, forming an hemispheric polyhedron, and with one or two oxygen atoms of the interslabs species. Each slab is made of two (100) layers of Th and P(1)O_4 units, like in the monazite structure (a rocksalt packing of M^{3+} cations and PO_4^{3-}tetrahedra). Nevertheless, in the title compounds, the tetrahedra have a different orientation and share only one edge with the other anionic polyhedra instead of two. Note that this edge is short, with a correlatively low O(11)–P(1)–O(11) angle (96.3(5)° for TPHPH).

On the Fourier maps, the 4 other phosphate groups in the cell (and the water molecules if any) appear scattered in the interslabs over equivalent 16*h* (general) positions of *Cmcm*, supposing a 1/4 occupancy rate. The case of each compound will be detailed below, the atomic coordinates are reported in Table 2.

3.1. TPHPH

The *Cmcm* space group precludes the interslab species from fully occupying their sites since the lowest site multiplicity (4) is twice the number of each of these units ($2HPO_4$ and $2H_2O$). Indeed, the Fourier maps show residual electrons on 16*h* sites of the interslabs, with densities corresponding to a 1/4 occupancy (experimentally: 0.253(2)). The ordering of the interslab is very probable because the phosphate sites strongly overlap each other, so that the presence of a unit forbids the occupation of the three nearest sites. The overlaps are also strong between these phosphates and the water molecules, leading to a unique array once a phosphate is placed in one of its four possible sites. For the example shown in Fig. 4, the unoccupied equivalent positions have been omitted, but they can be deduced through the missing symmetry elements, giving the three other possible arrays. The compactness of this packing results in an order that extends mechanically to the whole (*b*, *c*) interslabs layer, reducing its symmetry to a mere *c*-glide mirror.

However, the thickness of the slabs probably precludes any ordering interaction following *a*, consistently with the absence of superstructure diffraction peaks, as illustrated on the (010) projection (Fig. 5) and features an aperiodic random succession of the interslabs species. The position of

Table 2
Atomic coordinates and isotropic displacement factors for TPHPH, α-TPD and α-TPDH (in this order)

Atom	x	y	z	Site, occ.	B_{iso}[a], B_{eq} (Å^2) for Th
Th	0.36002(4)	0.6481(1)	1/4	8*g*, 1	1.40(4)
	0.35982(3)	0.64805(9)			0.78(2)
	0.35974(5)	0.6482(1)			0.58(2)
P(1)	0.18215(7)	0.6747(3)	1/4	8*g*, 1	1.3(1)
	0.18229(7)	0.6868(2)			1.14(8)
	0.18279(7)	0.6837(3)			0.7(1)
P(2)	0.5155(1)	0.6640(8)	0.5236(6)	16, 1/4	
	0.5098(3)	0.6459(8)	0.5463(6)		
	0.5109(3)	0.641(1)	0.5544(8)		
O(11)	0.1597(3)	0.8100(8)	0.0871(6)	16*h*, 1	0.5(1)
	0.1614(3)	0.8232(8)	0.0857(6)		0.17(8)
	0.1613(4)	0.815(1)	0.0832(7)		0.1(1)
O(12)	0.2539(1)	0.656(2)	1/4	8*g*, 1	
	0.2538(1)	0.661(1)			
	0.2541(1)	0.654(2)			
O(13)	0.1475(5)	0.4734(9)	1/4	8*g*, 1	
	0.1485(4)	0.4840(7)			
	0.1454(6)	0.487(1)			
O(21)	0.5549(3)	0.483(1)	0.552(2)	16*h*, 1/4	
	0.544(1)	0.455(2)	0.588(3)		
	0.539(1)	0.444(3)	0.611(4)		
O(22)	0.5359(5)	0.790(2)	0.362(2)	16*h*, 1/4	
	0.5379(9)	0.795(3)	0.409(2)		
	0.543(2)	0.760(4)	0.404(4)		
O(23)	0.4472(2)	0.6154(9)	0.511(1)	16*h*, 1/4	
	0.4475(6)	0.582(3)	0.471(4)		
	0.4476(8)	0.578(4)	0.486(5)		
OH	0.5219(9)	0.800(2)	0.712(2)	16*h*, 1/4	
O_b	1/2	0.753(1)	3/4	4*c*, 1/2	
O_b	1/2	0.762(2)	3/4	4*c*, 1/2	
O_w	0.4558(2)	0.1999(7)	0.568(2)	16*h*, 1/4	
	—	—	—	—	
	0.458(1)	0.144(5)	0.594(4)	16*h*, 1/4	

[a]Common for P(1) and P(2) on the one hand, and for all oxygen atoms on the other hand.

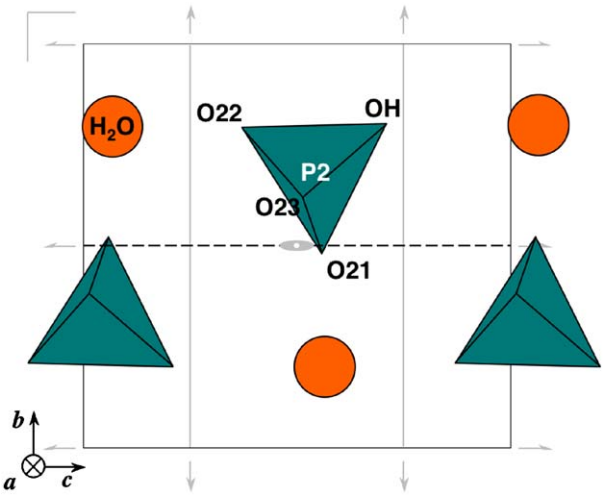

Fig. 4. One of the four possible arrays for the (100) interslab near $x = 1/2$ in TPHPH, featuring the *c*-glide plane at $y = 1/2$. Some of the lost symmetry elements of *Cmcm* are drawn in gray.

one of the interslabs oxygen atoms (OH), far from all thorium atoms ($d > 4$ Å) confirms the presence of hydrogenphosphate groups. During the refinement, soft constraints were applied on the P–O distances and O–P–O angles of this tetrahedron, considering K_2HPO_4 as a reference [15]. The water molecule appears surrounded by 7 oxygen (non-water) atoms (2.62 Å $< d O_w$–O < 3.20 Å) and one thorium atom.

Consequently to the reduction of symmetry in the interslabs, the unique thorium atom presents paradoxally two kinds of environments, notwithstanding the indirect effect on the neighbor $P(1)O_4$ tetrahedra: half (thereafter refered as Th/A) are bonded to O(23) of the HPO_4 unit and O_w of the water molecule while the other half (Th/B) is bonded to O(21) and O(22), leading in both cases to an 8-fold coordination. The ordering of the interslabs imposes that all thorium atoms standing on the same side of a slab belong to the same kind (A or B) and are different from those forming the other side. However, the disorder along *a* does not impose any correlation between the opposite sides of a slab.

The slight shift reported above when assuming two independent Th atoms in the *Cc* symmetry may be a consequense of that differenciation, although it seems difficult to correlate each position with the type (A or B) of environment. Indeed, the slab seems rigid enough to remain unsensitive to the drop of symmetry of the interslabs, allowing to consider mean positions for Th and $P(1)O_4$ in the refinements. It is also worth to note their quasi-invariance from TPHPH to α-TPD. The final esd's on Th and P(1) coordinates are low enough to validate this orthorhombic model. Indeed, no subgroup allows depicting correctly the occupation of many interslabs site, as observed on the Fourier maps. For example, extending the *Cc* symmetry to the whole structure by doubling the slab's atoms gives $R_{Bragg} = 0.053$ instead of 0.039 for *Cmcm*.

The bond strength calculation for Th, using Brese's model [16] (Table 3), shows a non-negligible contribution of the water molecule (0.29 valence units) that allows to fulfill the valence of Th/A. Moreover, the water molecules of TPHPH complete the coordination sphere of half of the thorium atoms and contribute to the stabilization of this compound.

The only known isotypes of TPHPH are its cerium and uranium counterparts, $Ce_4(PO_4)_4(HPO_4)_2 \cdot 2H_2O$ [17] and $U_4(PO_4)_4(HPO_4)_2 \cdot 2H_2O$ [18], which have similar cell parameters, respectively $a = 21.0142(3)$ Å, $b = 6.55082(7)$ Å, $c = 6.94382(6)$ Å, $\beta = 91.983(1)^\circ$, $V = 955.32(2)$ Å^3 and $a = 21.140(6)$ Å, $b = 6.600(4)$ Å, $c = 6.994(2)$ Å, $\beta = 91.67(6)^\circ$, $V = 975.4(6)$ Å^3, but are monoclinic $C2/c$. Therefore, the atoms ignore the special position on the *m*-mirror at $z = 1/2$. Their structure is very similar to that of TPHPH, but the lower overall symmetry results from a 50%-occupiedpositions in the interslabs instead of 25%.

The TPHPH cell already reported by Salvado et al. is monoclinic $P2_1$ (instead of orthorhombic *Cmcm*) [11]. The

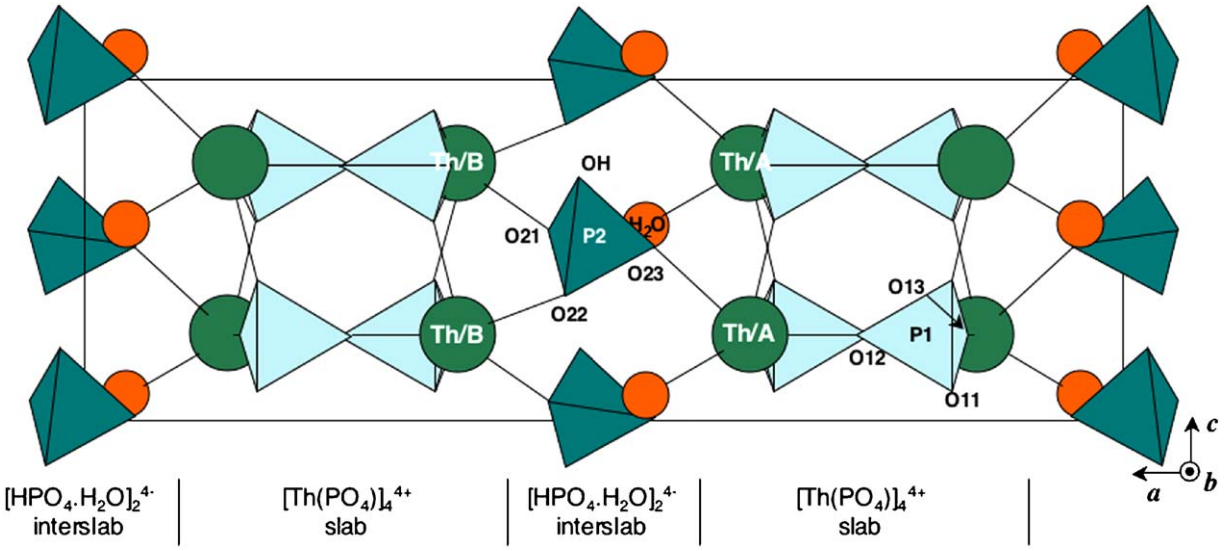

Fig. 5. (010) view of TPHPH. P–O distances (Å): P(1)–O(11) = 1.538(5) (2*x*), −O(12) = 1.541(3), −O(13) = 1.539(7), P(2)–O(21) = 1.493(8), −O(22) = 1.48(1), −O(23) = 1.502(5), −OH = 1.61(1).

Table 3
Th–O distances (Å) in TPHPH, α-TPD and α-TPDH. Cumulated bond strengths ($\Sigma_o s_o$ in valence units) are calculated from [16]

	TPHPH		α-TPD		α-TPDH	
	Th/A	Th/B	Th/A	Th/B	Th/A	Th/B
O(11) (2*x*)	2.573(6)	2.503(5)	2.557(6)			
O(11) (2*x*)	2.425(5)	2.411(4)	2.397(5)			
O(12)	2.275(2)	2.272(2)	2.262(3)			
O(13)	2.185(6)	2.254(5)	2.272(7)			
O(21)		2.453(9)	2.45(2)		2.45(3)	
O(22)		2.55(1)		2.65(2)		2.46(3)
O(23)	2.626(6)			2.48(2)		2.55(3)
O_w	2.625(8)				2.74(3)	
$\Sigma_o s_o$	*3.9*	4.2	*3.8*	4.1	*4.0*	4.1

monoclinic (m) and orthorhombic (o) cells can be linked as follows:

$$a_m = b_o;\ b_m = c_o;\ c_m = (a_o + b_o)/2;\ V_m = V_o/2.$$

Based upon an improper cell, this model ignores most of the symmetries, absent in the monoclinic system. Although the slabs of the TPHPH structure show a roughly similar array of Th and PO_4 units, these authors doubled each atom of the asymmetric unit. They also ignored the *m*-mirror perpendicular to c_o (i.e. b_m), therefore the special position of Th and P(1), although their atoms lie in the same $(010)_m$ plane. The resulting thorium polyhedra have odd open shapes, esd's on the Th–O distances are high and cumulated bond strengthes for the thorium atoms are worth 3.3 and 4.4. The array of the HPO_4 and H_2O units is strongly different from ours and ignores the disorder. Indeed, our preliminary X-ray studies inclined us to think that, even with the right cell, a structure with such extreme electron densities on atoms sites can hardly be resolved with a mere laboratory X-ray diffractometer.

3.2. α-TPD

Two hypotheses are consistent with the existence of only two P_2O_7 units in the *Cmcm* cell:

- the two tetrahedra of a diphosphate group are equivalent through either an *m*-mirror or a two-fold axis belonging to *Cmcm* and located on the bridging oxygen O_b, thus leading to a local *m* or 2 symmetry (an inversion center can be excluded according to a previous NMR study [9]);
- these tetrahedra are non-equivalent, leading to a 1 symmetry (in this case, all the non-trivial symmetry elements of *Cmcm* are lost).

Every possible symmetry reduction has been considered, but for steric reasons, the only realistic solution was to place the O_b atom on the *b*-directed two-fold axis of *Cmcm* (position 4*c*). This model also gave the lowest reliability factors. A resolution led with the second model resulted into a similar geometry. For the same steric reasons than for TPHPH, the P_2O_7 units necessarily order in the (*b*,*c*) planes (Fig. 6) in α-TPD, but probably not following the *a*-axis. The interatomic distances appear satisfactory (Table 3). Finally, the refined value of the interslabs sites occupation factor is close to 1/4 (0.244(3)), as for TPHPH, in agreement with the *Cmcm* symmetry.

The TPHPH/α-TPD transition requires the inversion of half of the HPO_4 tetrahedra, thus the breaking and reformation of some Th–O bonds in the interslabs. In these conditions, half of the Th/A become Th/B and reciprocally, leading to a new order consisting in an alternation of Th/A and Th/B atoms on the same side of a slab, contrarily to the TPHPH structure.

Th/B keeps the same environment than in TPHPH, but Th/A loses the neighbor water molecule, resulting in an open seven-fold polyhedron, with uncomplete cumulated bond strength for the cation. Soft constraints were applied to the P(2)–O distances and O–P(2)–O angles for the refinement. The P(2)–O_b–P(2) (non-constrained) linkage appears strongly bent (127.1(5)°), as usually observed in diphosphate groups. In a survey of the vibrational spectroscopy of anhydrous phosphates, Rulmont et al. correlate unambiguously the $\Delta v = (v_{as} - v_s)$ and $\Delta = (v_{as} - v_s)/(v_{as} + v_s)$ parameters derived from the stretching frequencies of 15 diphosphates to the P–O–P angles, in the 124–180° domain [19]. Once integrated into these plots, the Δv and Δ values calculated from the vibration observed on the μ-Raman or IR spectra of α-TPD at 250 °C ($v_s = 778\,cm^{-1}$, $v_{as} = 940\,cm^{-1}$) [9], account for a P–O–P angle around 123°. Data are scarce in this low-angle region of the Rulmont's plot, but as far as we can rely on them, the calculated value appears in good agreement with the result of the Rietveld analysis.

3.3. α-TPDH

As in the α-TPD structure, the symmetry of the interslabs appears reduced to the *b*-directed two-fold axis of *Cmcm*. The previous order/disorder considerations apply to this form, resulting in an array similar to that of the anhydrous form, with an additional water molecule positioned similarly as in TPHPH (Fig. 7). The refined value of the 16*h* interslabs sites occupation factor is 0.244(2).

The molecule is surrounded by another water molecule (2.85(4) Å), 6 non-water oxygen atoms ($2.61 < d$ O_w–$O < 3.06$ Å) and one thorium atom. Concerning the diphosphate groups, the bending of the P(2)–O_b–P(2) linkage (119.7(6)°) is still stronger than in α-TPD, even if this value must be considered carefully because of the low weight of the P_2O_7 group in the formula. To our knowledge, a lower angle has been observed only in α-$Na_2CuP_2O_7$ (118.6(2)°) [20], but it appears from the literature dealing with unprotoned diphosphates that the P–O–P angle for hydrated compounds (127° for 16 occurrences) is usually lower than for anhydrous ones (average value of 133°, for 63 occurrences, excluding angles of 180° resulting from a position disorder of diphosphates groups or highly anisotropic motion of O_b). Generally, a low angle is observed when the bridging oxygen atom is bonded to an external cation (i.e., Na-O_b = 2.426(2) Å in $Na_4P_2O_7$ [21]) or when a water molecule is close enough (2.6–3.1 Å) to form an hydrogen bond with it. α-TPDH

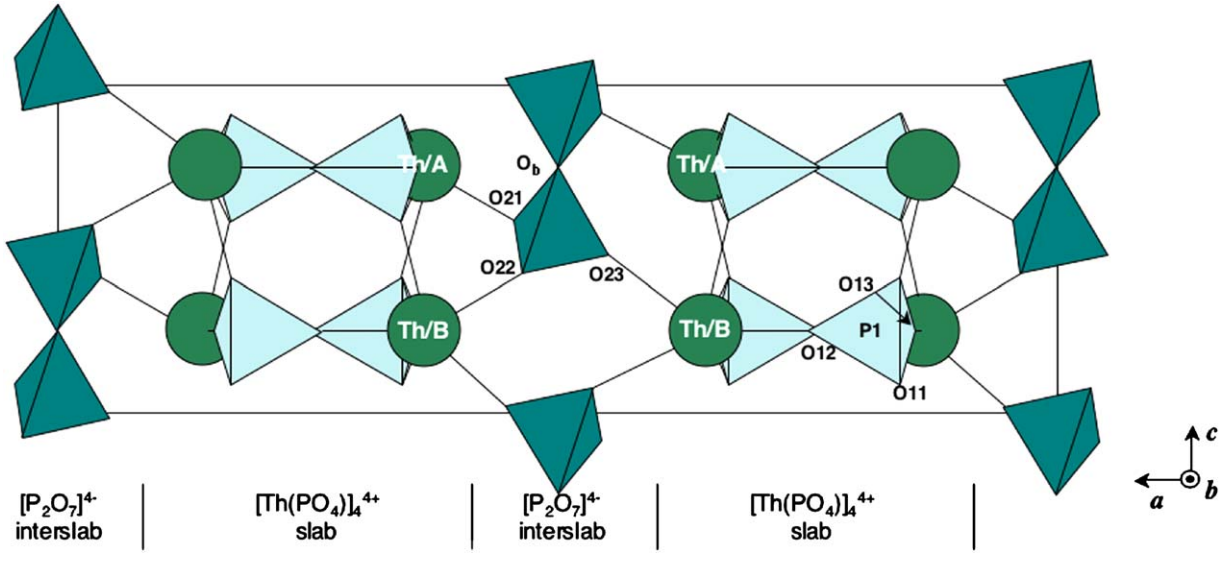

Fig. 6. (010) view of α-TPD. P–O distances (Å): P(1)–O(11) = 1.538(5) (2*x*), −O(12) = 1.542(3), −O(13) = 1.539(6), P(2)–O(21) = 1.50(2), −O(22) = 1.52(2), −O(23) = 1.50 (2), −O_b = 1.616(6).

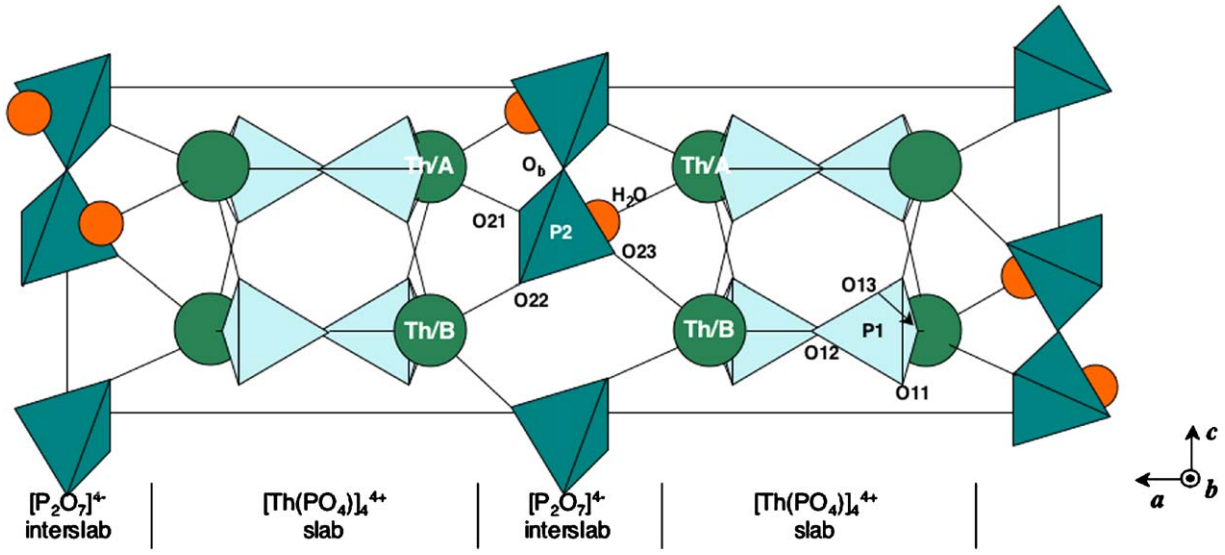

Fig. 7. (010) view of α-TPDH. P–O distances (Å): P(1)–O(11) = 1.537(6) (2*x*), −O(12) = 1.540(4), −O(13) = 1.539(9), P(2)–O(21) = 1.51(2), −O(22) = 1.50(3), −O(23) = 1.50 (2), −O_b = 1.613(8).

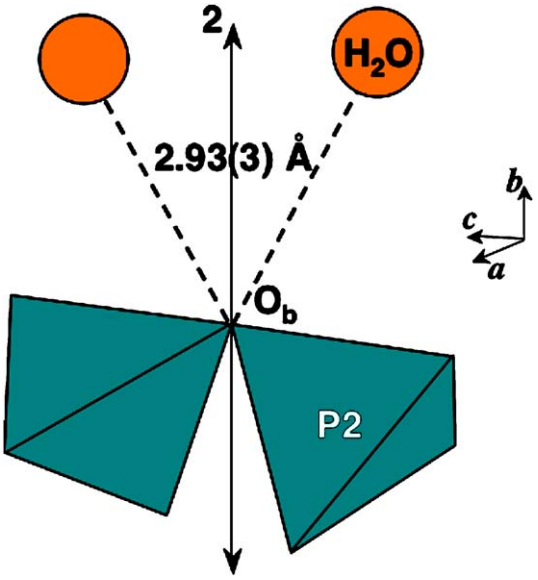

Fig. 8. The bending effect of the hydrogen bonds on the diphosphate unit of α-TPDH.

appears as an ideal case for such a distortion, with two water molecules near O_b (dO_w–O_b = 2.93(3) Å) and placed in such a manner that they can pull the bridging oxygen away from the P(2)–P(2) axis (Fig. 8).

4. Discussion

In spite of the evolution of the interslabs species, the $[Th_4(PO_4)_4]^{4+}$ slab remains remarkably unchanged between TPHPH, α-TPDH and α-TPD. In the three forms, the thorium atom shares about 3.3 valence units with the slabs oxygens, accounting for the stability of this pseudo-monazite array. On the opposite, the network of Th bonds with HPO_4 oxygens appears very weak, in agreement with the platelet habit of the TPHPH crystallites.

The water molecule in TPHPH and in α-TPDH plays a significant structural role by completing the coordination polyhedron of half of the thorium atoms. Its absence explains the tendency of α-TPD to re-hydrate promptly when left in air. The similar behavior of TPHP comes probably from the same origin. The *a*-parameter is only faintly sensitive to the presence of water since the interslabs are templated by the bigger HPO_4 or P_2O_7 units, however, the dehydration leaves wide cavities, as shown for α-TPD in Fig. 9.

The α-TPD/β-TPD transition near 950 °C consists in a break in the structural continuity that prevailed from room temperature up to this temperature. A structural explanation of this mechanism can be proposed by comparing the (001) projections of the two forms (Figs. 9 and 10). Let us observe, for example, the movements of two thorium atoms belonging to the same slab: in Fig. 9, Th/I is located in the mirror plane at $z = 3/4$ (upper level), Th/II at $z = 1/4$ (lower level). After shifting parallel to the (010) plane at $y = 1$, following the arrows, these atoms can be found again in Fig. 10. Note that Th/I and Th/II, now at the same $z = 3/4$ (upper) level, have become non-equivalent in the process. In a more general way, the transformation occurs via a $\pm(a/8–c/4)$ alternate shearing, occurring in the (010) planes with integer *y*'s of the α-cell. The flat slabs of α-TPD sustain an enormous deformation (see dashed lines) and the empty cavities of the interslabs disappear, thus explaining the reduction of 5% of the unit cell volume per formula. The transverse shearing requires the breaking and reformation of some intra-slabs Th–O bonds, but the densification of the framework allows the formation of new inter-slabs bonds (asterisked in Fig. 10). On the contrary, the *c*-parameter, corresponding to the thickness of two layers remains almost unchanged (+0.5%).

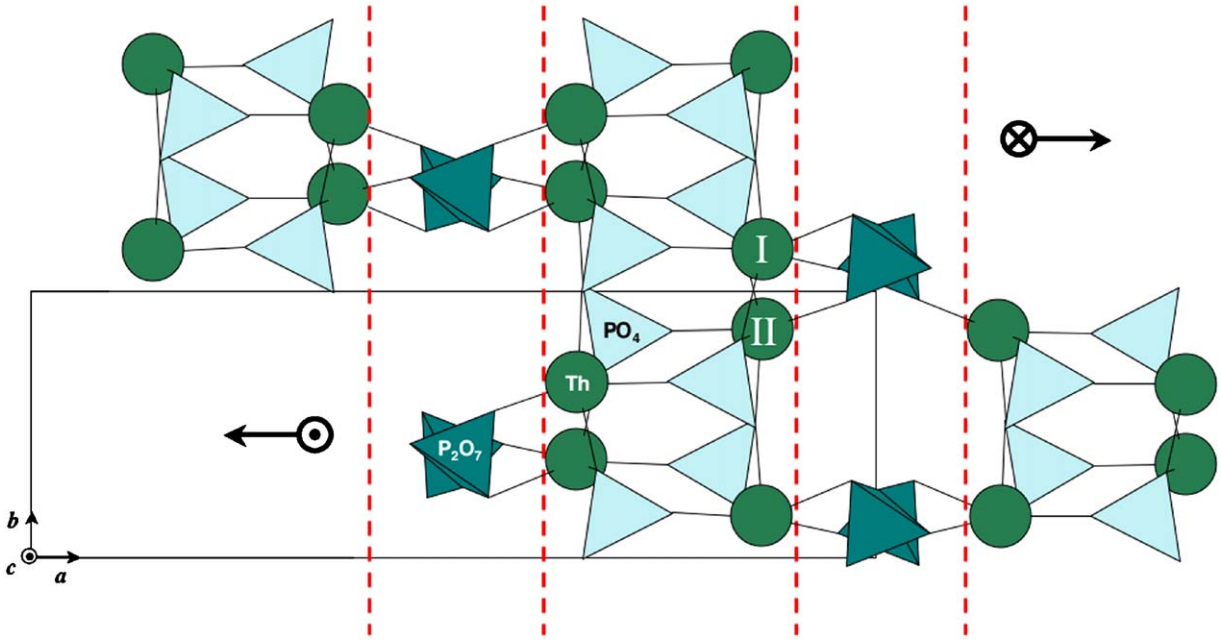

Fig. 9. (001) view of α-TPD. The arrows feature the shearing leading to β-TPD.

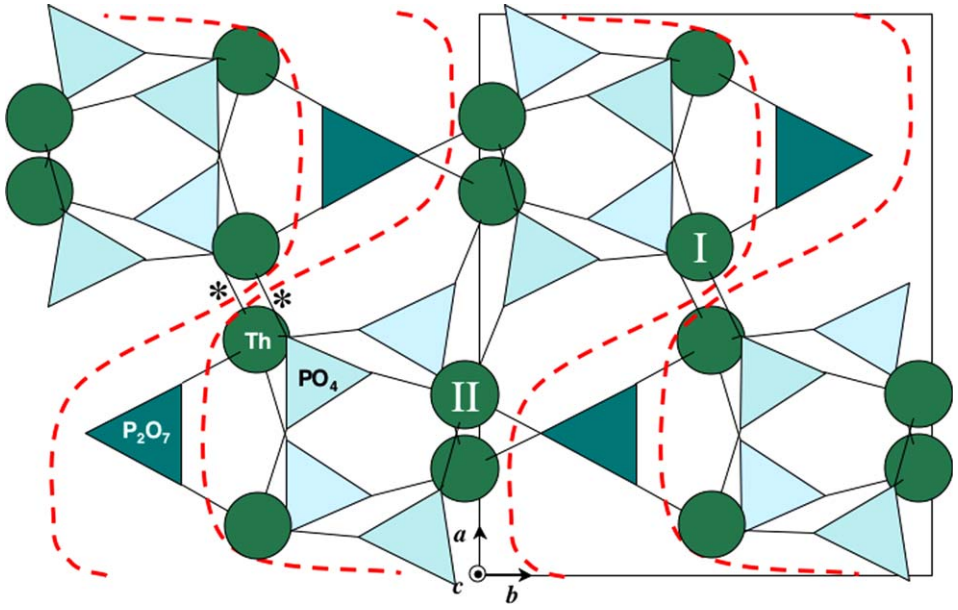

Fig. 10. (001) view of β-TPD, showing the same atoms as in Fig. 9. Note the reduction of the interslabs cavities and the corrugated shape of the slabs, now linked by the asterisked bonds.

Finally, the P_2O_7 units realign along the *c*-axis of β-TPD. Nevertheless, their random array along the *c*-directed P_2O_7 chains, previously observed by single-crystal XRD and NMR [10] can now be described as a remanence of the initial disorder of the interslabs species in TPHPH, TPHP, then in α-TPD.

While α-TPD appears as a 2D compound, β-TPD is nearly 3D and can be grown as regular-shaped crystals instead of platelets. This point is of considerable importance in the field of the sintering properties mentioned for β-TPD ceramics. However, the location of Th atoms in irregular polyhedra at the surface of the slabs allows regarding important substitutions for this cation, because variations of the ionic radius of the tetravalent cation can be absorbed by slight deformations of the framework. Indeed, the flexibility of the corrugated slabs has been evidenced in the frame of a dilatometric study [22].

The absence of cavities in β-TPD and the cumulated bond strengths of 4.1 and 4.3 around the thorium atoms explain why the ultimate form is immune from rehydration, at variance with α-TPD and TPHP. Furthermore, the collapse of the structure justifies the exothermal

character of the transition: α-TPD, unstable in standard conditions because of its tendency to re-hydrate, becomes metastable at high temperature, until the thermal energy becomes sufficient to activate the first-order transition and stabilize the thorium atoms by forming inter-slabs bonds. In both cases, the necessity to complete the coordination polyhedron of Th by filling or reducing the cavities appears as a thermodynamic necessity.

The other positive point resulting from the structure collapse is the compactness of the framework of the β-form, that offers a better resistance to the water penetration, in agreement with the excellent performance of this material in terms of leaching and solubility [3].

5. Conclusion

The present study now allows understanding how, starting from a soft and foliated precursor, β-TPD achieves its remarkable stability towards temperature, water and other aggressive media after a series of thermal evolutions affecting first the interslabs, then the slabs themselves through an irreversible and exothermal transition.

These criteria are of considerable importance with regard to its applications as a host material for the long-term storage of actinides. Several additional experiments are carried out carefully in the field of the immobilization of tetravalent actinides (such as uranium, neptunium or plutonium). First, in order to develop such a way of preparation, the incorporation of the given actinides in TPHPH must be efficient. This important aspect was already checked for uranium which forms solid solutions of formula $Th_{4-x}U_x(PO_4)_4(HPO_4)2\cdot 2H_2O$ (TUPHPH) [18]. By this way, the final β-TUPD ceramics exhibit high resistance to aqueous alteration consequently to a significant improvement of the homogeneity in the cations distribution compared to that observed by using dry or other wet chemical processes. Additional experiments dealing with the formation of $Th_{4-x}Np_x(PO_4)_4(HPO_4)_2\cdot 2H_2O$ (TNpPHPH, $x\leqslant 2$) and $Th_{4-x}Pu_x(PO_4)_4(HPO_4)_2\cdot 2H_2O$ (TPuPHPH, $x\leqslant 4$) solid solutions also allowed to form β-TNpPD and β-TPuPD after heating at high temperature [23]. The behavior of the material under irradiation (including recoil nucleus and α particle produced by decay) is also examined [24] in the field of immobilization of tetravalent actinides. While the daughter products of ^{238}Pu, ^{239}Pu, ^{240}Pu, ^{242}Pu isotopes (uranium and thorium isotopes produced by successive α decays) could be stabilized in their tetravalent oxidation state, ^{241}Pu produces ^{241}Am then ^{237}Np through a β–α decay sequence. As already mentioned, ^{237}Np could be immobilized in β-TNpPD solid solutions. On the contrary, as already reported, americium (or curium) could be incorporated with maximum weight loading of 1 wt%. Consequently, in order to immobilize higher americium rates, the preparation, sintering and chemical durability assessment of β-$TAn^{IV}PD/(An^{III},Ln)$-monazite composite materials are also carried out [25].

Acknowledgments

This work was supported by the French research group NOMADE (GdR 2023, CNRS/CEA/COGEMA, NOuveaux MAtériaux pour les DEchets,). The authors are very grateful to Jean-Paul Souron (Université Paris VI, France) for the DTA/TGA experiments.

Appendix A. Supplementary Materials

Supplementary data associated with this article can be found in the online version at doi:10.1016/j.jssc.2006.05.027.

References

[1] J.-C. André, C. R. Acad. Sci. Paris IIA 333 (2001) 835.
[2] N. Dacheux, N. Clavier, A.-C. Robisson, O. Terra, F. Audubert, J.-E. Lartigue, C. Guy, C. R. Acad. Sci. Paris 7 (2004) 1141.
[3] A.-C. Thomas, N. Dacheux, P. Le Coustumer, V. Brandel, M. Genet, J. Nucl. Mater. 281 (2000) 91.
[4] A.-C. Thomas, N. Dacheux, V. Brandel, P. Le Coustumer, M. Genet, J. Nucl. Mater. 295 (2001) 249.
[5] A.-C. Robisson, N. Dacheux, J. Aupiais, J. Nucl. Mater. 306 (2002) 134.
[6] V. Brandel, N. Dacheux, M. Genet, Radiokhimiyia 43 (2001) 16.
[7] V. Brandel, N. Dacheux, E. Pichot, M. Genet, J. Emery, J.-Y. Buzare, R. Podor, Chem. Mater. 10 (1998) 345.
[8] V. Brandel, N. Dacheux, M. Genet, in: Procédés de préparation d'un produit à base de phosphate de thorium et/ou d'uranium (IV) en vue de la décontamination d'effluents radioactifs, Patent 03739522.5-2111-FR0300426, 2003.
[9] V. Brandel, N. Clavier, N. Dacheux, J. Emery, M. Genet, G. Wallez, M. Quarton, Mater. Res. Bull. 40 (2005) 2225.
[10] P. Bénard, V. Brandel, N. Dacheux, S. Jaulmes, S. Launay, C. Lindecker, M. Genet, D. Louër, M. Quarton, Chem. Mater. 8 (1996) 181.
[11] M.A. Salvado, P. Pertierra, A.I. Bortun, C. Trobajo, J.R. Garcia, Inorg. Chem. 44 (2005) 3512.
[12] J. Rodriguez-Carvajal, FULLPROF.2k: Rietveld, profile matching and integrated intensity refinement of X-ray and neutron data, V 1.9c, Laboratoire Léon Brillouin, CEA, Saclay, France, 2001.
[13] G.M. Sheldrick, SHELX-97: A Program for Crystal Structure Determination, Göttingen, Germany, 1997.
[14] J. Gonzalez-Platas, J. Rodriguez-Carvajal: GFOURIER: Fourier maps calculation program, V 3.20, Universidad de La Laguna, Tenerife, Spain, Laboratoire Léon Brillouin, CEA, Saclay, France, 2003.
[15] T. Lis, Acta Crystallogr. C 50 (1994) 484.
[16] N.E. Brese, M. O'Keeffe, Acta Crystallogr. B 47 (1991) 192.
[17] M. Nazaraly, G. Wallez, C. Chanéac, E. Tronc, F. Ribot, M. Quarton, J.-P. Jolivet, Angew. Chem. 44 (2005) 5691.
[18] N. Clavier, N. Dacheux, G. Wallez, M. Quarton, J. Nucl. Mater. (2006) available online.
[19] A. Rulmont, R. Cahay, M. Liègeois-Duyckaerts, P. Tarte, Eur. J. Solid State Inorg. Chem. 28 (1991) 207.
[20] F. Erragh, A. Boukhari, F. Abraham, B. Elouadi, J. Solid State Chem. 120 (1995) 23.
[21] K.Y. Leung, C. Calvo, Can. J. Chem. 50 (1972) 2519.
[22] S. Launay, G. Wallez, M. Quarton, Chem. Mater. 13 (2001) 2833.
[23] J. Rousselle, in: Etude de la formation de PDT en milieu nitrique en vue d'une décontamination d'effluents de haute activité contenant des actinides, Ph.D. Thesis, Université Paris-Sud-11, IPNO-T-04-03, 2004.
[24] N. Clavier, N. Dacheux, R. Podor, Inorg. Chem. 45 (2006) 220.
[25] C. Tamain, A. Özgümüs, N. Dacheux, F. Garrido, L. Thome, J. Nucl. Mater. (2006) (in press, available online).